Investigation of the Motion of Relativistic Electrons

Vedang Lad, Bryan Sperry*
MIT Department of Physics
(Dated: January 28, 2022)

We use an enclosed magnetic field and vacuum to measure the velocity of decaying Strontium (^{90}Sr) atoms by changing the voltage between plates on a velocity selector. Following a calibration using the known Barium energy spectrum (^{133}Ba) we then extract the kinetic energy and velocity of the traveling electrons. We find an electron energy-mass density value of 583 ± 108 keV using the relativistic model and 1963 ± 108 keV using the Newtonian model.

I. INTRODUCTION

Relativity has successfully described the motion of high-speed particles over 100 years now. As first described by Einstein in [2] "On the Electrodynamics of Moving Bodies", the theory states that the laws of physics and the speed of light are the same in all inertial reference frames. This means that unlike classical mechanics, the speed of light can never be greater than that 299,792,458 $\frac{\text{m}}{\text{s}}$.

We utilize ejected electrons produced by Strontium as it decays to Yttrium. This form of beta decay is known to produce electrons moving approximately at 60%-70% of the speed of light. [1] We control the trajectory of the electrons using a magnetic field and a velocity selector. This trajectory forces the electron to hit the PIN diode detector which registers voltage pulses to an amplifier and eventually to a multi-channel analyzer (MCA). A barium calibration is performed in order to map voltage pulses to energy values, from which we extract kinetic energy, velocity, and momentum of the particles. We represent the data through Newtonian and relativistic models and determine which represents the motion of the electrons best.

II. THEORETICAL REMARKS

II.1. Newtonian and Relativistic Dynamics

In Newtonian dynamics we characterize the momentum $\vec{p}$ and the velocity $\vec{v}$ and the mass m using the relationship and the kinetic energy as [1]

$$\vec{p} = m\vec{v} \tag{1}$$

$$K = \frac{p^2}{2m} \tag{2}$$

The theory of relativity introduces the Lorentz factor $\gamma = \frac{1}{\sqrt{1-\beta^2}}$ where $\beta = \frac{v}{c}$. This factor appears in the relativistic "version" of equation 1 and equation 2,

$$\vec{p} = \gamma m\vec{v} \tag{3}$$

$$K = (\gamma - 1)mc^2 \tag{4}$$

$$= mc^2(\sqrt{1 + (\frac{p}{mc})^2}) \tag{5}$$

Lastly, we have the Lorentz force law which places a key role behind the physics of the velocity selector in the presence of a magnetic field $\vec{B}$ and electric field $\vec{E}$ which is described by $F = q(\vec{E} + \frac{\vec{v}}{c} \times \vec{B})$ where we take q to be the charge of the electron, denoted as e from now on. Note that the Lorentz force laws apply in both relativistic and Newtonian physics.

II.2. Experimental Theory

There are two different regions on the the apparatus as seen in figure 1. There is a region with just a magnetic field and another region with a magnetic field and an electric field (the velocity selector). The force and momentum of an electron due to the magnetic field is described by the equation

$$\vec{F} = \frac{mv^2}{\rho} = \frac{ev\vec{B}}{c} \tag{6}$$

$$\vec{p} = \frac{ev\vec{B}}{\rho} \tag{7}$$

where ρ is the path radius as seen in figure 1. This is obtaining by equating the centripetal force and the Lorentz force law equation II.1. The velocity selector is where $\vec{F}_{electron} = 0$. Setting the Lorentz force law to zero we have that

$$v = \frac{Ec}{B} \tag{8}$$

$$\beta = \frac{E}{B} \tag{9}$$

This is the same β referenced in an earlier section and essential for the data analysis that follows in section II.1. We can then rewrite all of our equations in terms of β.

* vedlad@mit.edu; http://web.mit.edu/8.13/

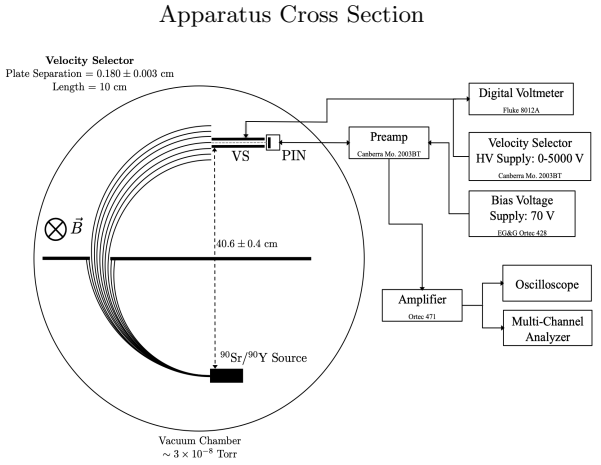

FIG. 1. The electron leaves the $^{90}Sr/^{90}Y$ source and follows a circular path due to the magnetic field present. It passes through the velocity selector and experiences an electric force before it strikes the PIN diode. Many electrons get filtered out by the aperture and the velocity selector. The boxes show voltage controllers that control the fields present and amplifiers that display pulses on the MCA

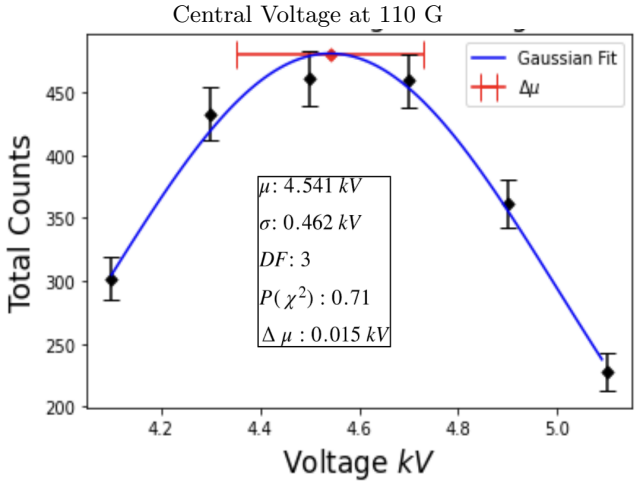

FIG. 2. The calculated central voltage in red with corresponding error bars which were obtained from the fit. Error-bar on other points are extracted from the MCA and assigned Poisson errors. The blue line depicts a Gaussian fit with $P(\chi^2) = 0.71$

This is the same β seen in 8. We have that

$$\beta_{Classical} = \frac{eB\rho}{mc^2} \tag{10}$$

$$\beta_{Relativistic} = \frac{eB\rho}{mc^2\sqrt{1+(\frac{eB\rho}{mc^2})^2}} \tag{11}$$

$$\beta_{Experimental} = \frac{E}{B} = \frac{V_{Central}}{Bd} \tag{12}$$

III. EXPERIMENTAL ARRANGEMENT

Our apparatus consisted of spherical housing surrounded by copper coils which generate the magnetic field. As seen in the cross-section in figure 1, high-speed electrons emitted from the decay follow a circular path and first encounter a baffle or an aperture. They continue to the velocity selector and strike the PIN diode. Here the pulse on the diode passes through the pre-amplifier, amplifier, and is ultimately recorded on the MCA. The strength of the magnetic field and the voltage between the plates are controlled independently.

III.1. Calibration

We perform a two-day barium calibration on the first day. This is in order to have recorded counts at higher energies on the energy spectrum. All other days we perform a short fifteen-minute calibration. As seen by figure 4 the long barium calibration results in distinct peaks that have known energy values[1]. These will be linearly mapped to the energies of ejected electrons, seen in a subsequent section.

III.2. Central Voltage Determination

The central voltage is determined using a two-pass approach. The first pass is to estimate the central voltage. This is done by increasing the voltage between the plates in large increments. After each increment, we record data for one minute. From an estimate on the central voltage in the first pass, we perform finer increments before and after the central voltage for two minutes. We save files on the MCA with the discriminator set to channel 65 in order to filter out low-energy noise. We repeat aforementioned steps for 80 G, 90 G, 95 G, 100 G, 105 G, 110 G.

After calculating the central voltage, we save two-minute runs at the central voltage from each magnetic field. Since the central voltage represents when the electric and magnetic forces are balanced seen by II.1, we extract the most information from the dynamics of the electron.

IV. DATA AND ANALYSIS

IV.1. Central Voltage and Charge-Mass Ratio

We calculate the central voltage for a given magnetic field by summing all of the counts for a given voltage. We then plot the sum and fit a Gaussian to the data as seen in figure 2. We take the mean value of the Gaussian

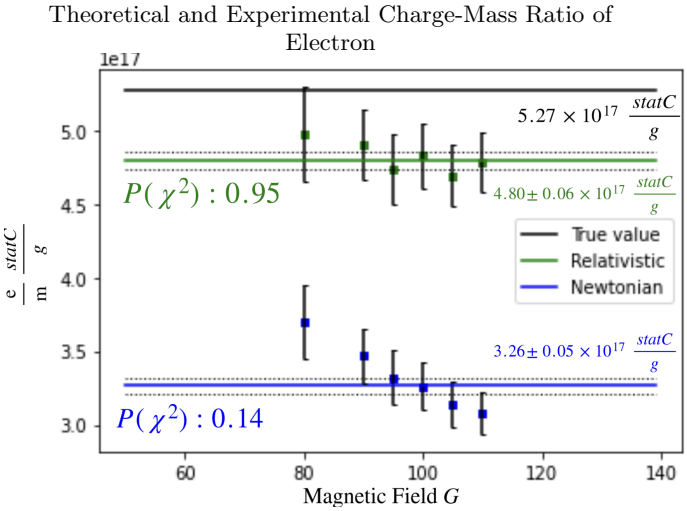

FIG. 3. The green line represents the relativistic equation in section 10 while the blue represents the Newtonian equation in section 10. The theoretical line is seen in the black line on top of the plot. The errors on the points are propagated by the red error bars in the figure 2. We obtain error bars through 20,000 Monte Carlo simulations. The Newtonian points which decrease with the magnetic field are not representative of a constant fit unlike the relativistic.

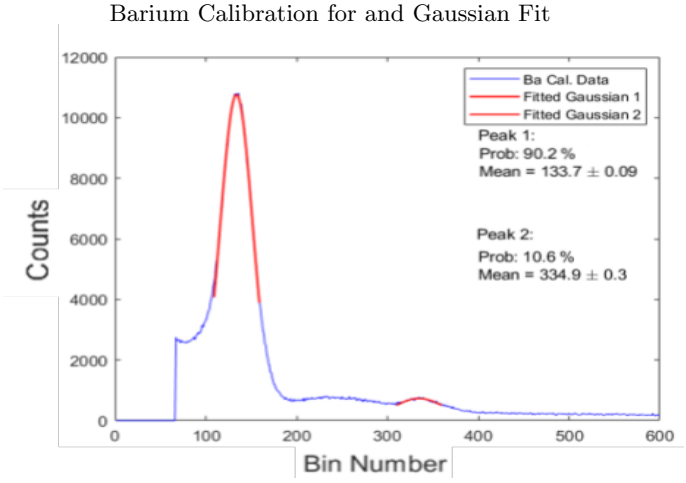

FIG. 4. This is the 15 minute calibration obtained the day of data collection. The two distinct peaks which correspond to 30.97 KeV 81 keV are then fit with Gaussian to extract the MCA channel. These are linearly fit to obtain a channel to energy conversion.

as the value of the central voltage. The error of the mean value is extracted from the fit. While the fit need not be a Gaussian, the average P(χ^2) across all magnetic fields was 0.27. Furthermore, the mean of the Gaussian allows simple extraction of the peak value.

To extract the charge-to-mass ratio we substitute the third equation of 10 into the first two and rewrite them in terms $\frac{e}{m}$. This results in the following:

$$(\frac{e}{m})_{Classical} = \frac{V_{Central}c^2}{B^2 d\rho} \tag{13}$$

$$(\frac{e}{m})_{Relativistic} = \frac{V_{Central}c^2\sqrt{1+(\frac{V_{Central}}{Bd})^2}}{B^2 d\rho} \tag{14}$$

The plot that results from this relationship can be seen in figure 3. As seen in the plot, the relativistic line is significantly closer to the theoretical value that the Newtonian line. Furthermore, the constant fit does not represent the linear decrease that is characterized by the blue points, furthermore suggesting a relativistic dependence on the electron dynamics. We obtain errors on the constant fits through Monte Carlo simulations. The Monte Carlo simulation randomly displaces the central voltage up to σ and then performs a new constant fit. The standard deviation across all simulations is then taken as the uncertainty of the fit.

IV.2. Calibration and Energy

We perform the Barium calibration in order to isolate the charge and the mass of the electron from the data. We fit a Gaussian to the peaks generated by the spectrum, as seen in figure 4. Similar to the reasoning behind the central voltage, the peaks need not be Gaussian but the Gaussian fits allow easy extraction of the mean channel value and uncertainty from the fit quality of the fit. We then use the obtained points to a linear fit of the form the linear relation: $E = \alpha n + \beta$ where E is the energy and the n is the channel. We find that $\alpha = 0.249 \pm 0.007$ $\frac{\text{eV}}{\text{bin}}$ and $\beta = -2.29 \pm 0.002$ eV. Here we take the uncertainty from the fit. Using this, we can now convert the peak channels to the corresponding peak energies.

As seen in figure 5, we plot the kinetic energy using theoretical Newtonian 1 and relativistic 3 model as well as the experimental model. There is a vertical offset between the theoretical and experimental values. While the shape of the experimental data is linear like the relativistic model, its energy off from about a factor of $\frac{1}{2}$. This offset shows the shortcomings of the barium calibration. During the barium calibration, the distance from source-to-detector is smaller than electrons ejected by ^{90}Sr. This offset may cause calibrated electrons to be at lower energies than which may explain the vertical offset.

The final step as seen in figure 6 we extract the slope from a linear fit. Here, the kinetic energy is plotted against $(1-(\frac{E}{B})^2)^{\frac{-1}{2}} - 1$. The slope here represents the electron energy mass density mc^2, as seen in equation 10. While we show only the relativistic value in figure 6, the Newtonian model had a slope of 1963 ± 108 keV with a P(χ^2) = 0.87. The theoretical value of the electron energy mass density, 511 keV, lies 1σ outside the rela-

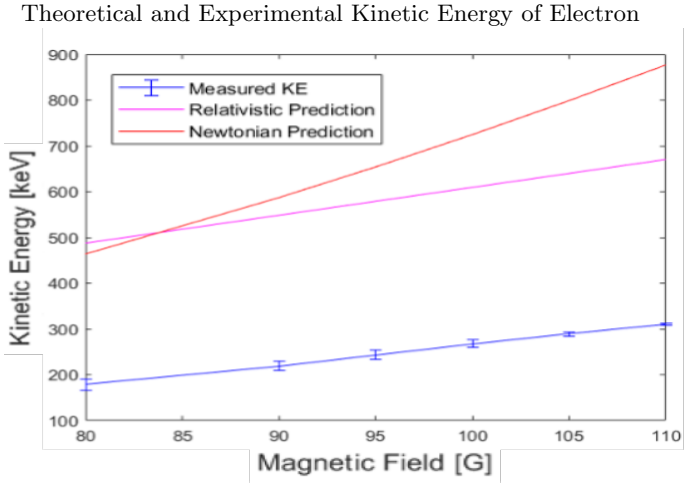

FIG. 5. The pink line represents the theoretical relativistic equation 1 while the red represents the theoretical Newtonian equation 3. The experimental line is the blue line. There is a vertical offset between the theoretical and experimental due to uncertainties in the barium calibration. The experimental data is parallel to the relativistic value, suggesting a relativistic correspondence regardless of the vertical offset.

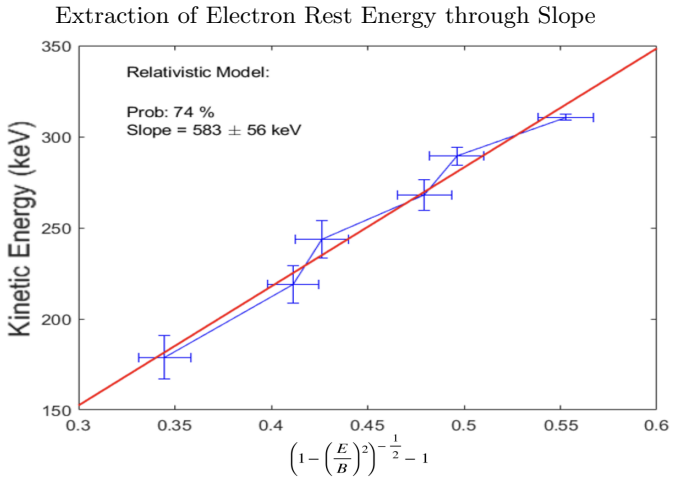

FIG. 6. The blue line represents a trivial interpolation between the points drawn to characterize the linear relationship. A P(χ^2)=0.74 suggests a good linear fit. Notice we propagate uncertainties in both x and y which come from the barium calibration and the central voltage determination respectively. This fit suggests a slope of 583 ± 56 keV

tivistic model and outside 13σ of the Newtonian model. 1σ uncertainty is dominated by the same barium calibration uncertainty that we see in figure 5. Experimental and theoretical values are more consistent with the Newtonian model than the relativistic.

IV.3. Uncertainties

While apparatus contents are sealed in the vacuum, we follow the uncertainties prescribed in [1]. We have that:

$\sigma_\rho = 0.4$ cm	2%
$\sigma_d = 0.4$ cm	2%
$\sigma_G = 1.14$ G	5%

We obtain systematic uncertainties, ρ and d, by perturbing the fitting parameters up to σ and noting the change in the energy-mass density. To factor in the non uniformity of the magnetic field, we measure the field at different points and take the deviation from the mean as the uncertainty. Other uncertainties arise from energy loss due to Coulomb scattering and the PIN diode result in trivial uncertainties. Statistical uncertainties mains rise from the fact that electron decay and incidence is a random process. We propagate this along with voltage and magnetic field uncertainties through the data analysis to obtain the final energy-mass density.

V. SUMMARY

Experimental data presented strongly suggests that the relativistic model represents electrons moving at 60% to 70% of the speed of light better than the Newtonian model. We see uncertainties arise largely through the barium calibration with adds an offset to the energies. Longer daily calibration that reveals more peaks in the spectrum would help correct this issue. From the experimental data, we find an electron rest density of 583 ± 56 $(stat.)$ ± 52 $(sys.)$ keV using the relativistic model which is within error of the true value of 511 keV. This is unlike the Newtonian which we find 1963 ± 108 $(stat.)$ ± 176 $(sys.)$ keV, suggesting correctness of the theory of relativity within uncertainty.

ACKNOWLEDGMENTS

We gratefully acknowledge the help of Sean Robinson, Xiaowei Ou, Professor Paus for generously granting an extension and lastly Albert Einstein for his genius.

[1] J. L. Staff, Optical Trapping guide (2018), jLab E-Library, URL http://web.mit.edu/8.13/www/JLExperiments/JLExp51.pdf
[2] Einstein, A. (1905). On the Electrodynamics of Moving Bodies. Annalen Der Physik, 891–921.
[3] P. Bevington and D. Robinson, Data Reduction and Error Analysis for the Physical Sciences (McGraw-Hill, 2003).